

Fast Two-photon Microscopy by Neuroimaging with Oblong Random Acquisition (NORA)

Esther M. Whang

*Department of Biomedical Engineering
Center for Imaging Science
Johns Hopkins University
Baltimore, MD 21218.*

EWHANG2@JHU.EDU

Skyler Thomas

*Department of Biomedical Engineering
Johns Hopkins University
Baltimore, MD 21218.*

STHOM215@JHU.EDU

Ji Yi

*Department of Biomedical Engineering
Wilmer Eye Institute
Kavli NDI
Johns Hopkins University
Baltimore, MD 21218.*

JYI@JHU.EDU

Adam S. Charles

*Department of Biomedical Engineering
Center for Imaging Science
Mathematical Institute for Data Science
Kavli NDI
Johns Hopkins University
Baltimore, MD 21218.*

ADAMSC@JHU.EDU

Abstract

Advances in neural imaging have enabled neuroscience to study how the joint activity of large neural populations conspire to produce perception, behavior and cognition. Despite many advances in optical methods, there exists a fundamental tradeoff between imaging speed, field of view, and resolution that limits the scope of neural imaging, especially for the raster-scanning multi-photon imaging needed for imaging deeper into the brain. One approach to overcoming this trade-off is in computational imaging: the co-development of optics and algorithms where the optics are designed to encode the target images into fewer measurements that are faster to acquire, and the algorithms compensate by inverting the optical image coding process to recover a larger or higher resolution image. We present here one such approach for raster-scanning two-photon imaging: Neuroimaging with Oblong Random Acquisition (NORA). NORA quickly acquires each frame in a microscopic video by subsampling only a fraction of the fast scanning lines, ignoring large portions of each frame. NORA mitigates the loss of information by extending the point-spread function in the slow-scan direction to effectively integrate the fluorescence of neighboring lines together into a single set of measurements. By imaging different, randomly selected, lines at each frame, NORA diversifies the information content across frames and enabling a video-level reconstruction. Rather than reconstruct the video frame-by-frame using an image-level recovery algorithm, NORA recovers full video sequences through a nuclear-norm minimization (i.e., matrix completion) on

the pixels-by-time matrix. We simulated NORA imaging using the Neural Anatomy and Optical Microscopy (NAOMi) biophysical simulation suite. Using these simulations we demonstrate that NORA imaging can accurately recover $400 \mu\text{m} \times 400 \mu\text{m}$ fields of view at subsampling rates up to 20X, despite realistic noise and motion conditions. As NORA requires minimal changes to current microscopy systems, our results indicate that NORA can provide a promising avenue towards fast imaging of neural circuits.

1. Introduction

Discovering principles of neural computation at the cellular level rests on the ability to record large populations of signal cell’s activity. Two-photon microscopy enables the imaging of activity at a large scale deep within the tissue while maintaining high spatial resolution, resulting in its popularity within neuroscience. For standard multi-photon microscopes, the effective speed of such standard systems enable scanning of reasonably large FOVs (0.5-1 mm square FOVs) at approximately 30 Hz. However, while $\approx 30\text{Hz}$ is sufficient for capturing dynamics from calcium indicators, the framerate is currently insufficient for capturing fast neural dynamics such as from voltage indicators, which requires at minimum $\times 10$ increase in frame rate to effectively record. The restriction on the frame rate arises due to how two-photon microscopes acquire images, a process called raster-scanning in which the field-of-view (FOV) is scanned point-by-point. Due to this scanning method, two-photon microscopy faces a trade-off between temporal and spatial resolution: improving the frame-rate requires reducing the amount of samples acquired per frame resulting in poorer spatial resolution, but fully sampling a field of view lowers the frame rate. Imaging a larger area imposes further restrictions on the temporal and spatial resolution.

Addressing this resolution-area-speed tradeoff is incredibly important in increasing the size of our window into neural dynamics and has thus prompted numerous approaches for high-speed, large-scale imaging (Wu et al., 2021). Most approaches develop purely optical designs that spread light across the tissue (Lu et al., 2017, Song et al., 2017, Demas et al., 2021). Examples include volumetric imaging via Bessel beams (Lu et al., 2017) or stereoscopic imaging (Song et al., 2017), multiplane imaging through various forms of beam-splitting (Demas et al., 2021), and ROI-specific sampling (Mattison et al., 2023). Computational imaging methods, which utilize the co-design of hardware and software, have become another way to address the tradeoff between frame rate and spatial resolution (Kazemipour et al., 2019). While effective, these methods all require collecting light from each fluorescing object in the field-of-view (FOV). Given that the power constraints on *in vivo* imaging systems and the scattering nature of the tissue, spreading the light too much will quickly reduce signal-to-noise levels beyond recoverability and thus effectively cap the maximum effective improvement of such approaches. Furthermore, many of these methods are vulnerable to motion artifacts due to the need for pre-established structural priors, restricting the generalizability of such systems.

We present here an ultra-fast two-photon microscope that overcomes the speed-resolution-area tradeoff. Our method, Neuroimaging by Oblong Random Acquisition (NORA), only requires simple hardware and well-studied optimization-based reconstruction methods. It utilizes randomized line-by-line subsampling and an elongated point spread function (PSF) to efficiently encode measurements at each frame. In particular, light is not assumed to be collected from the full field-of-view, enabling much larger speed-ups by simply skipping portions of each frame. From the subsampled-and-blurry measurements, the full recording then can be reconstructed by posing the recovery as a matrix completion problem (Candes and Plan, 2010), leveraging the low-rank nature inherent to multi-photon videos. Crucially, instead of considering each frame of measurement in isolation, NORA considers the measurements as a whole across both its spatial and temporal components. Throughout the entire pipeline, there is no need for complicated optical components or *a-priori* information about the imaging target, not to mention extensive computational resources.

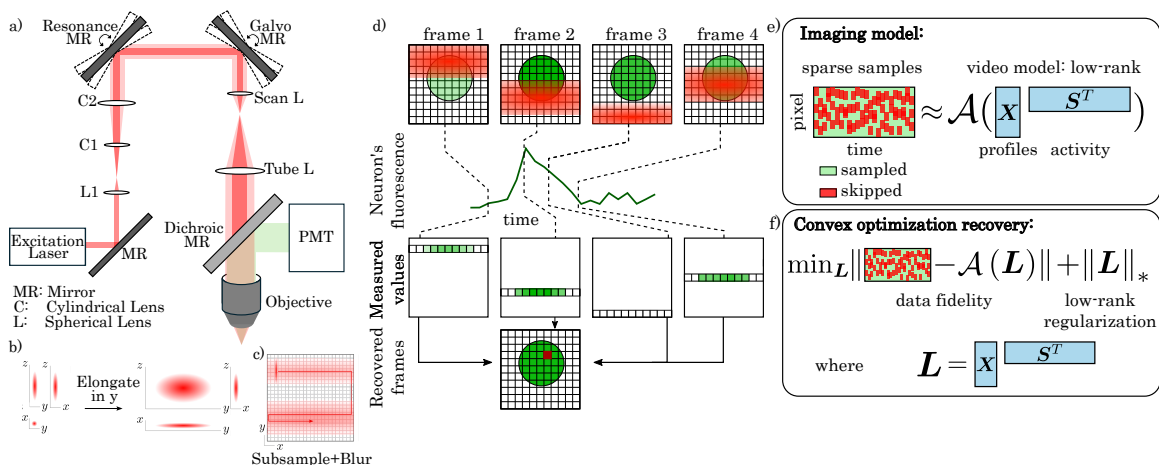


Figure 1: Overview of NORA design. a) the proposed design for the NORA microscope, which is the standard two-photon microscope with the addition of two cylindrical lenses to achieve an elongated PSF. b) Elongated PSF shape used in the NORA design. c) Example sampling pattern depicting the blur-and-subsample approach. d) Schematic depicting the recovery process. A single pixel is integrated in multiple wide-line scans. The combined information over multiple frames, along with the correlations between frames, provides enough information to triangulate the value of the single high-resolution pixel at all frames. e) The imaging model quantifies the optical path as a blur operator applied to a low-rank fluorescence video matrix, followed by a sub-sampling operator. Importantly, all operations in the forward model are linear. f) The recovery process solves a nuclear-norm regularized least-squares optimization. This optimization finds the video that both matches the observed samples and the *a priori* model of fluorescence video being low-rank.

We demonstrate the capabilities of the NORA pipeline by utilizing an advanced two-photon microscopy simulator (Song et al., 2021). We show that with NORA, it is possible to achieve two-photon recordings with up to 1/20th of the original raster lines even with realistic obstacles such as noise and motion. From the combined design of simple optical changes and holistic data recovery, NORA address a significant bottleneck in increasing the frame-rate of two-photon microscopes, enabling possible applications with larger FOVs and faster indicators.

2. NORA System Design

At a high level, our design is a combined modification to the optical scanning schedule combined with an algorithmic back-end that reconstructs the partially sampled data (Fig. 1). The optical front-end design seeks to minimize the time spent per frame by reducing the number of lines acquired. This approach leverages the fast resonant galvos used in typical 2P designs while still reducing the total sampling needed to sample each image. The back end is based on matrix completion, an estimation approach that can leverage correlations in both space and time at once.

2.1 Data Acquisition

The Neuroimaging by Oblong Random Acquisition (NORA) data acquisition works as thus: For every frame, an elliptical excitation beam randomly line-scans a fraction of the entire field-of-view. The sampled lines are intentionally selected to be different at each frame, with the goal diversifying the information captured between concurrent frames (by avoiding imaging the same locations). The

elliptical PSF is elongated only in the slow-scan direction, covering the area that is equivalent to several raster-lines in a traditional two-photon microscope. Crucially, while the excitation beam is elongated along the slow scan axis, it is not elongated to the point that it accounts for all of the unsampled lines. Furthermore, lines are not spaced out to prevent overlaps, meaning that lines closer than the elongation length may both be collected in the same frame. Each frame will thus have unsampled areas, parts of the field-of-view that are not captured at that time point by any line.

The random line subsampling directly enables the imaging speedup, as the time to acquire each frame is proportional to the number of lines scanned. However, at the subsampling scale of NORA, subsampling with a standard gaussian PSF is insufficient due to how much of the image remains unsampled. When the number of sampled lines become increasingly small, a simple subsampling-only system would pose a significant limit on the total amount of information that could be acquired. The oblong PSF serves to partially account for unsampled lines by illuminating the lines directly surrounding each scanned lines, collecting fluorescence signal from tissue that otherwise would have been passed over. The signal is collected all at once, effectively summing together the neighboring lines, weighted by the elliptical PSF intensity decay. The ability to acquire signals from multiple lines simultaneously through the elliptical PSF allows for a further reduction in the number of raster lines required per frame while still effectively capturing that frame’s information from our target.

Mathematically we can consider the observed measurements as coming from a forward model that consists of two stages, each of which is well modeled by a linear operator. If we denote the “true” image at time t that would have been acquired with a slower scan as \mathbf{X}_t , the result of the NORA optical design can be described by first applying a blur operator through a convolution as $\mathbf{b} * \mathbf{X}_t$, where \mathbf{b} is the two dimensional representation of the elliptical point-spread function. We can consolidate notation by vectorizing the frame at time t as a single vector \mathbf{x}_t rather than a 2D image, and we can define an equivalent matrix \mathbf{B} such that the blurring operation is a simple matrix multiple $\mathbf{B}\mathbf{x}^1$. Given the blurred version of the image, the measurements are simply the selection of some of the resulting values. We denote this operation as \mathbf{S} , which is an $M \times N$ matrix of zeros and ones where each row has a 1 only in the column corresponding to a collected measurement. The recorded data for image t , which we denote \mathbf{y}_t is thus

$$\mathbf{y}_t = \mathbf{S}_t \mathbf{B} \mathbf{x}_t + \epsilon, \tag{1}$$

where ϵ represents the observation noise. Note that \mathbf{S}_t is time-dependent as the samples collected for each image in the video sequence are different.

The resulting subsampled-and-blurry measurements will still have missing information from the target if each frame is seen in isolation, despite the elliptical beam ameliorating the amount of information lost. This loss is mitigated by the design choice of selecting different randomly selected lines at different frames. Thus areas not captured on a frame at time t are likely to be captured at frames in time $t - 1$, $t + 1$, etc. It is then up to the reconstruction algorithm to leverage these diverse measurements across multiple frames to not just deblur the lines that were collected with the spread PSF, but to fill in the missing areas using information shared *between* frames.

2.2 Computationally Recovering Missing Measurements

Given the subsampled measurements, NORA recovers the video by leveraging the strong spatial and temporal correlations in two-photon microscopy videos of neural activity. Specifically, NORA uses the specific mathematical model that fluorescence microscopy data is low-rank. Rank refers to the number of linearly independent rows or columns in a matrix. If a matrix has a rank significantly lower than its dimensions, then it is referred to as low-rank. One of the useful properties of low-rank matrices is that they can be decomposed from a high-dimensional form into much smaller matrices

1. We note that \mathbf{B} has a complex 2-level block circulant structure, however the form of \mathbf{B} is not important as all that matters is that we can apply the blurring operation to any image. This application can be done in the image domain as a convolution, and the notation here is simply for mathematical efficiency.

(Fig. 1e is one such example). The more compact representation of the data makes low-rankness particularly useful in the case of big datasets or large language models, where small and simple approximations are much needed (Bell and Koren, 2007, Hu et al., 2021).

In the context of microscopy data, if we consider all frames as vector $(\mathbf{x}_1, \mathbf{x}_2, \dots)$ concatenated into a pixels-by-time matrix ($\mathbf{X} = [\mathbf{x}_1, \mathbf{x}_2, \dots, \mathbf{x}_T] \in \mathbb{R}^{N \times T}$), we can safely assume that the rank of \mathbf{X} is $R \ll \min(N, T)$. To understand the low-rank assumption, consider a sequence of frames: In any sequence, any particular frame is likely to be similar to its preceding frames. Specifically, each frame should capture the same anatomical object, simply with slightly different fluorescence levels per object at each time (refer to the first row of Fig. 1.d, where the profile is simply changing in intensity). The shared information between frame greatly reduces the effective complexity of the data, enabling a low-rank model for fluorescence microscopy data. This has been successfully done for denoising and segmentation (Buchanan et al., 2018, Mukamel et al., 2009, Benisty et al., 2022), but utilizing low-rank to recover the $N \times T$ video from fewer observations is still under-explored.

The NORA recovery algorithm utilizes a low-rank prior to reconstruct a full video from under-sampled measurements. To understand the algorithm, we first recall the mathematical representation of our data acquisition pipeline and extend the per-frame forward model (Equation (1)) to a model over a sequence of frames.

$$\mathbf{Y} = \mathcal{A}(\mathbf{X}) + \mathbf{E} = \mathbf{S}(\mathbf{B}\mathbf{X}) + \mathbf{E}, \quad (2)$$

where here $\mathbf{S}(\cdot)$ is the linear sampling operator that returns for the k^{th} column (i.e, the blurred k^{th} frame) the samples (lines) taken for that frame, and \mathbf{E} is the $M \times T$ measurement error matrix. Note that here $\mathbf{S}(\cdot)$ is not a matrix but an operator since each frame is sampled with a different pattern. Thus, while $\mathbf{S}(\cdot)$ is still linear, it cannot be written as a single matrix that can be applied to all frames, as \mathbf{B} can. $\mathbf{Y} \in \mathbb{R}^{M \times T}$ denotes our observed measurements, where each column is the set of M blurry measurements selected at that frame. $\mathbf{X} \in \mathbb{R}^{N \times T}$ likewise represents the original imaging target across time.

With a model of how the observed measurements are acquired, it becomes possible to recover the imaging target (a full, non-blurry video) by inverting the forward model. However, this inversion is a non-trivial problem. Despite the model being linear, using a direct pseudo-inverse is not possible due to the fact that $MT < NT$. The under-determined nature of the inverse problem means that an infinite number of solutions exist. To compensate for the incomplete measurements, we use the prior knowledge of the low-rank model.

We frame, as in much of the computational imaging and inverse problem literature, the high-level goal of determining an estimate $\widehat{\mathbf{X}}$ that satisfies both our observed measurements and our *a priori* model of low-rank fluorescence video. Imposing this a-priori constraint enables us, as it has had in many other applications, the recovery of \mathbf{X} despite the ill-conditioned form of the forward model. Mathematically we find the estimate $\widehat{\mathbf{X}}$ through the nuclear-norm formulation of low-rank matrix completion (Fig. 1f), i.e., we optimize the cost function

$$\widehat{\mathbf{X}} = \arg \min_{\mathbf{X}} \|\mathbf{Y} - \mathbf{S}(\mathbf{B}\mathbf{X})\|_F^2 + \|\mathbf{X}\|_*, \quad (3)$$

where the first term is the data fidelity term in the form of a Frobenius norm that enforces the estimate to match the observed samples across all frames, and the second term is the nuclear norm (defined as the sum of singular values of the matrix) that prioritizes low-rank solutions. Solving this optimization has been well studied in the literature. For our implementation, we selected an efficient first-order optimizer that is readily available (Becker et al., 2011).

Our easy-to-implement design eliminates many of the difficulties associated with high-speed two-photon microscopy such as cost and expertise. Both the data acquisition and reconstruction aspects of NORA solely rely on simple changes to pre-existing structures. The hardware design of the NORA system is remarkably similar to the traditional two-photon system, only requiring an addition of a

cylindrical lens pair to achieve the elongated point spread function (Li et al., 2024). Likewise, the reconstruction does not rely on algorithmically complicated and expensive steps such as model pre-training or gathering large training datasets. These two components taken together removes major barriers towards ultra-fast microscopy.

3. Results

3.1 Validation through Simulation

We validate our design through simulation of our NORA optical path in a biophysical simulation suite followed by reconstruction using the matrix completion approach (Fig. 2). We simulated the subsampled-and-blurry measurements through the NAOMi simulator, a MATLAB-based two-photon microscopy simulator that can create highly-realistic movies of neural tissue with full ground truth (Song et al., 2021). It is important to emphasize that in our simulation, we do not simply take pre-recorded videos and apply the forward model $\mathcal{S}(\mathbf{B})$. Rather, NAOMi simulates the full 3D point-spread function and imaging pathway, inclusive of motion, sensor-realistic noise, etc. Using these realistic simulations, we generated a $400 \mu\text{m}$ by $400 \mu\text{m}$ by $100 \mu\text{m}$ volume of tissue mimicking the anatomy of mouse layer 2/3 in area V1 at $250 \mu\text{m}$ depth with GCaMP6f. The volume was fully scanned with an elongated PSF (FWHM of $1.15 \mu\text{m}$ by $3.35 \mu\text{m}$ by $6.99 \mu\text{m}$) at 120 mW power and 30 Hz frame rate over 1000 frames. The resulting blurry video was then subsampled by taking random columns from each frame.

We simulated scans with realistic nuisance variation, including noise and motion, as validated in the original NAOMi paper. We tested different levels of subsampling by undersampling the same video at 10X, 15X and 20X (i.e., 1/10th, 1/15th, and 1/20th of the total lines, respectively). Moreover, while we included tissue motion to simulate the most realistic settings, we further tested the impact of motion by comparing the results to the same video generated with the motion “turned off”.

We developed the reconstruction algorithm in MATLAB², utilizing the the Templates for First order Conical Solvers (TFOCS) library to solve a modified matrix completion problem (Becker et al., 2011). TFOCS offers several advantages, including only needing to compute the application of the measurement operator and its transpose, and the ability to use implicit functions (i.e., not needed to write out the linear operators as explicit matrices). These advantages greatly mitigate the general computational challenges of recovering entire video sequences by limiting the RAM and compute needed to run the solver.

3.2 Video recovery from NORA samples

Following the NORA pipeline, we simulated the NORA subsampling and blurring for different subsampling ratios: 1/10th, 1/15th, and 1/20th of the FOV. In Figure 3 we highlight example frames from the NORA-reconstructed videos, using frames from a fully-sampled scan with gaussian PSF (a traditional two-photon setup) as comparison. In these images we do not include any denoising to highlight the base spatial reconstruction capabilities of NORA.

Despite the extreme subsampling, the NORA reconstructions recover the frames to a visual quality on par with the traditional two-photon scan. We note that the reconstruction also shows no artifacts that could be associated with the line-subsampling - there are no distinct bands of missing information, only complete frames of activity. NORA also manages to maintain a surprising amount of consistency between the reconstructions from different subsampling ratios. As seen through the example frames, there are no major differences between the 1/10th subsampling reconstruction and the 1/20th subsampling reconstruction.

2. Code for both simulation and reconstruction will be released with the publication of this paper.

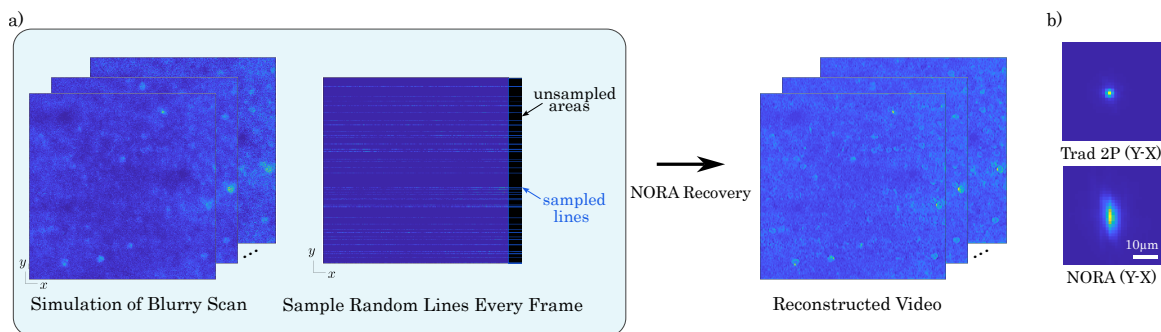


Figure 2: NAOMi simulation of NORA imaging. a) NAOMi simulates a full 3D volume of tissue *in silico*, which is then imaged with the desired PSF through an optics model that includes tissue-based aberration and photonic variability. The result is a blurry image of the tissue at each frame. Biophysical models of neural activity ensure realistic changes in fluorescence for the simulated neurons and processes, as well as for neuropil. Frame-specific sampling then selects the per-frame lines to keep, which are then inverted through the matrix completion recovery to obtain an estimate of the videos. Simulations through NAOMi enable the recovered video to be compared to “standard” imaging obtained through simulating a video sequence on the same volume and activity, but with a typical PSF and no subsampling. b) Example PSF used in the NAOMi simulation (bottom) compared to a traditional 2P PSF (top).

One point of concern was NORA’s robustness to motion. Rigid motion can increase the rank of a video matrix, challenging the use of the low-rank assumption of the NORA method due to how it breaks the alignment between frames, thereby increasing the effective rank of the matrix. To test the capacity of NORA to motion, we leveraged the ability of the NAOMi simulation framework to simulate both line-by-line and rigid motion). Figure 3a,b shows that despite these concerns, NORA is robust to motion, with the addition of motion only having a minor affect on the visual quality of the reconstructed videos. While some information, such as the overall sharpness of the reconstruction, is affected, the relevant information that would be needed for automated ROI, such as the location and size of each neuron, are successfully recovered in both the no-motion and motion cases. These test demonstrate that even though increased motion do impact the overall sharpness of the reconstruction, high levels of signal recovery are still possible up to 20X speedups. This suggests that although motion does increase the effective rank, the increase is not to the extent that the low-rank model no longer holds.

While the reconstructed videos demonstrated good pixel level image recovery, practical applications in neuroimaging require that the reconstructions from NORA must accurately capture the temporal activity of individual ROIs in the FOV. If the neural fluorescence fluctuations are distorted, then the imaging method is not well suited to scientific imaging. To examine the temporal traces, we compared the ground truth traces provided from the NAOMi simulator with the ROI time-traces extracted from the NORA reconstructions. We extracted the ROI traces by masking each reconstructed video with the ground truth spatial profile provided by NAOMi, i.e., the Profile-Assisted Least Squares (PALS) baseline (Song et al., 2021) (Fig. 4a). This choice removed possible confounds of algorithmic-specific accuracy levels, as well as the related artifacts such as false positive transients (Gauthier et al., 2022). To reduce noise and focus on signal recovery, we further median filtered all videos with a small 3D window (9x9x9) before traces were extracted. This process was critical for excluding extreme values that result from the Poisson-Gaussian nature of the simulated PMT noise. As a second point of comparison we also compared the NORA recovered ROI traces to traces from the traditional two-photon simulation scan. This comparison provided a reference for how well a typical system would have captured the ground truth activity. All traces shown

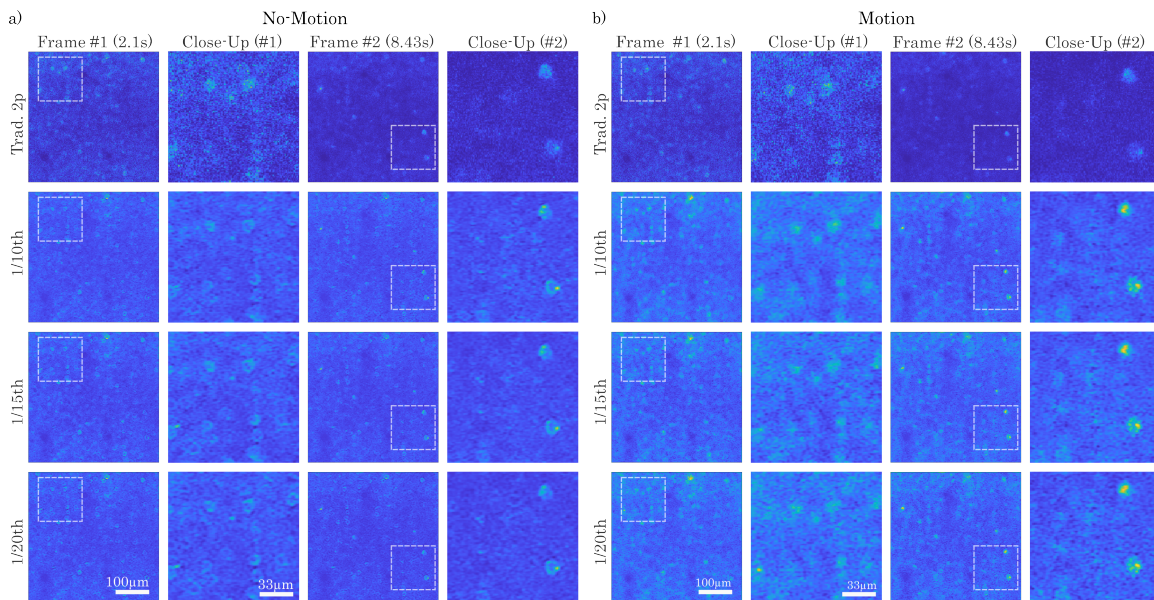


Figure 3: Spatial recovery results for NORA imaging using NAOMi simulations with no motion (a) and with motion (b). (a) and (b) both show example single frames and insets from using (from top to bottom) a traditional 2P PSF, NORA imaging at 10X, 15X, and 20X speedups ($1/10^{th}$, $1/15^{th}$, and $1/20^{th}$ of the lines per frame, respectively). While (a) maintains a slightly higher level of spatial resolution, individual cells are still clearly identifiable up to NORA at 20X for both cases.

in Figure 4b,c,d,e are for 33.33s of simulated recording. Figure 4b,d are from simulations without motion, while Figure 4c, e are from simulations with motion.

The traces extracted from the reconstructed volumes are largely in line with the traces from the ground truth for both the cases with and without motion (Fig. 4b,c). Traces such as #1, #3, and #6 show the consistency in the spike between the ground truth and the reconstruction. In cases like trace #7 in Figure 4c, where the reconstructed traces are not in line with the ground truth, we can see that the traditional two-photon traces also fail to follow the ground truth traces, suggesting that the failure is due to a general scanning issue rather than the NORA pipeline.

One important question we consider is the general trend of the reconstructions: do most traces consistently align with the ground truth, or a select special few? To verify the overall alignment of the extracted traces with the ground truth, the distribution of the correlation between the ground truth traces and the extracted traces are plotted in Figure 4d,e. Even in the simulation condition that includes motion, all traces from the reconstructed volumes show a skew toward the left, indicating a general trend of high correlation with the ground truth despite the inclusion of noise and motion in the measurement process.

4. Discussion

In this work we present NORA: a framework for fast imaging of raster-scanning two-photon imaging. NORA is based on a subsample-and-blur optical design combined with a matrix-completion recovery approach. The advantages of our system are 1) the simplicity of the optical design, 2) the use of both spatial and temporal statistics for video recovery, and 3) theoretical guarantees on recovery. Moreover, NORA uses generic low-rank statistics and thus does not require any training data or model fitting to perform the recovery.

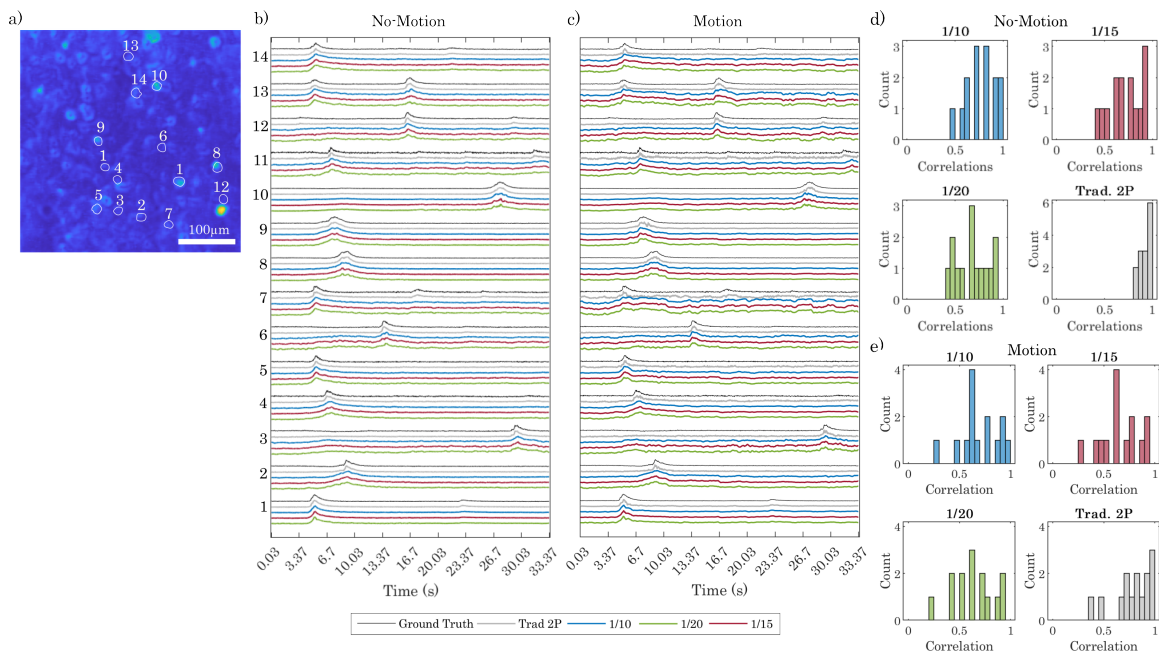


Figure 4: Temporal activity recovery results for NORA imaging. a) Standard deviation image of the median filtered reconstruction with circled ROIs representing individual neurons with significant activity, as identified from NAOMi simulator. Time traces from for the ROIs in panel (a) are shown in (b) for simulations without motion and (c) for simulations with motion. In both (b) and (c), activity is preserved up to 20X speedups. (d) and (e) show histograms of correlations between each imaging method and the ground truth time-traces used to generate the data from the NAOMi simulation for the cases with motion and without motion. While traditional 2P imaging has the highest correlations, the drop in correlations are minimal, indicating well-reserved neural activity.

One major feature to underscore is NORA’s remarkable robustness to both extreme subsampling and motion. As rigid motion increases the effective rank of a matrix by mis-aligning pixels at different time-points, we anticipated requiring additional algorithmic improvements to address motion. This increase in rank, however, was not as extreme with respect to the reconstruction as expected, and we were able to continue to reduce the number of measurements up to a 20X subsampling. The successful recoveries thus highlights one of the strengths of NORA, its capability to handle realistic variations that arise in most imaging devices.

In our approach with low-rank priors, we focused on traditional matrix completion based reconstruction that leverages nuclear norm minimization that has been highly successful in other statistical recovery domains (Candes and Plan, 2010, Charles et al., 2017, Ahmed et al., 2013). This approach moves from thinking of recovery as per-image frame-by-frame recovery to using the full set of spatial and temporal statistics. Moreover, these priors are powerful enough that reconstruction is possible without strong trained priors learned by ML deep learning approaches that have become more prominent. We thus bypass the need for training data, and remove the possibility of realistic hallucinations that can be difficult to diagnose. Furthermore, our recovery has the capacity to generalize to new tissue samples, unlike deep learning approaches which face significant out-of-distribution challenges in generalizing even across labs (Mishne and Charles, 2024).

Interestingly, many ROI detection algorithms are based on low-rank matrix factorization (Charles et al., 2022, Mishne and Charles, 2019, Giovannucci et al., 2019) (see Benisty et al. (2022) for a recent review with more examples). It is therefore an interesting future direction to consider

merging the ROI detection with the NORA reconstruction, saving computational effort and reducing possibilities of introducing artifacts through multiple stages of analysis. In this work, however, we focus on reconstruction as in enables all users to apply their specified ROI detection algorithms. Moreover, different cell types (e.g., astrocytes) or imaging targets (e.g., dendrites) require different ROI detection schemes (Mi et al., 2024, Charles et al., 2022) to address their respective challenges, further justifying video reconstruction as a first step.

In its physical implementation, the current design proposed for NORA only requires simple optical components. One aspect, however, that may differ from the simulation is the implementation of the random sampling scheme. Currently in the simulation, each frame of measurements consists of randomly selected columns. However, if this is directly implemented in a physical system, it would require the galvanometer to constantly change its acceleration to accommodate the varying distances between samples. This inconsistency could cause problems such as jerk, slowing down the system. A more preferable sampling scheme would consist of uniform distances between each sample, much like evenly-spaced columns of measurements, which would allow for consistent speed between each column of measurements. While the simulation for this work focused on fully random sampling, the flexibility of the NORA system allows for this type of sampling scheme, as long as each set of measurements is sufficiently different from its neighboring frames.

With NORA’s simple and practical design, our goal is to enable many labs to build an ultra-fast microscope with with minimal additional parts and microscope alignment. Our design simply requires trivial modifications to existing microscopy methods, making it simple to implement. We envision two possible use cases for the achieved speedup: fast imaging of a single FOV, and interleaved imaging of multiple FOVs. In the first, more obvious, use case a single FOV is sampled as fast as possible, using the full framerate to acquire signals that are much faster than calcium dynamics (e.g., voltage or neurotransmitter based indicators). This use case has a multitude of applications in studying neural interactions based on spike timing, where the ability to resolve events tied to individual spikes is critical. The second use case a random access refocusing element can be used to select multiple FOVs over the optically accessible extent and depth. This will allow calcium imaging data to be acquired in 10-20 independently selected FOVs (more the achievable number in other designs) that do not require that the planes be geometrically tied to each other (e.g., tiling in depth, as required in current designs). The second use case opens up the ability to study the network-level activity of multiple brain areas at the single neuron resolution.

Acknowledgments

EW and JY were funded by NIH award R01EB034272. ASC was in part funded by CZI award CP2-1-000000704.

References

- Ali Ahmed, Benjamin Recht, and Justin Romberg. Blind deconvolution using convex programming. *IEEE Transactions on Information Theory*, 60(3):1711–1732, 2013.
- Stephen R. Becker, Emmanuel J. Candès, and Michael C. Grant. Templates for convex cone problems with applications to sparse signal recovery. 3(3):165–218, 2011. ISSN 1867-2949, 1867-2957. doi: 10.1007/s12532-011-0029-5. URL <http://link.springer.com/10.1007/s12532-011-0029-5>.
- Robert M. Bell and Yehuda Koren. Lessons from the netflix prize challenge. 9(2):75–79, 2007. ISSN 1931-0145, 1931-0153. doi: 10.1145/1345448.1345465. URL <https://dl.acm.org/doi/10.1145/1345448.1345465>.

- Hadas Benisty, Alexander Song, Gal Mishne, and Adam S. Charles. Data processing of functional optical microscopy for neuroscience, 2022. URL <https://arxiv.org/abs/2201.03537>. Version Number: 1.
- E. Kelly Buchanan, Ian Kinsella, Ding Zhou, Rong Zhu, Pengcheng Zhou, Felipe Gerhard, John Ferrante, Ying Ma, Sharon Kim, Mohammed Shaik, Yajie Liang, Rongwen Lu, Jacob Reimer, Paul Fahey, Taliah Muhammad, Graham Dempsey, Elizabeth Hillman, Na Ji, Andreas Tolias, and Liam Paninski. Penalized matrix decomposition for denoising, compression, and improved demixing of functional imaging data, 2018. URL <http://biorxiv.org/lookup/doi/10.1101/334706>.
- Emmanuel J Candes and Yaniv Plan. Matrix completion with noise. *Proceedings of the IEEE*, 98(6):925–936, 2010.
- Adam S Charles, Dong Yin, and Christopher J Rozell. Distributed sequence memory of multi-dimensional inputs in recurrent networks. *Journal of Machine Learning Research*, 18(7):1–37, 2017.
- Adam S Charles, Nathan Cermak, Rifqi O Affan, Benjamin B Scott, Jackie Schiller, and Gal Mishne. Graft: Graph filtered temporal dictionary learning for functional neural imaging. *IEEE Transactions on Image Processing*, 31:3509–3524, 2022.
- Jeffrey Demas, Jason Manley, Frank Tejera, Kevin Barber, Hyewon Kim, Francisca Martínez Traub, Brandon Chen, and Alipasha Vaziri. High-speed, cortex-wide volumetric recording of neuroactivity at cellular resolution using light beads microscopy. *Nature Methods*, 18(9):1103–1111, 2021.
- Jeffrey L Gauthier, Sue Ann Koay, Edward H Nieh, David W Tank, Jonathan W Pillow, and Adam S Charles. Detecting and correcting false transients in calcium imaging. *Nature methods*, 19(4):470–478, 2022.
- Andrea Giovannucci, Johannes Friedrich, Pat Gunn, Jérémie Kalfon, Brandon L Brown, Sue Ann Koay, Jiannis Taxisdis, Farzaneh Najafi, Jeffrey L Gauthier, Pengcheng Zhou, et al. Caiman an open source tool for scalable calcium imaging data analysis. *elife*, 8:e38173, 2019.
- Edward J. Hu, Yelong Shen, Phillip Wallis, Zeyuan Allen-Zhu, Yuanzhi Li, Shean Wang, Lu Wang, and Weizhu Chen. LoRA: Low-rank adaptation of large language models, 2021. URL <http://arxiv.org/abs/2106.09685>.
- Abbas Kazemipour, Ondrej Novak, Daniel Flickinger, Jonathan S Marvin, Ahmed S Abdelfattah, Jonathan King, Philip M Borden, Jeong Jun Kim, Sarah H Al-Abdullatif, Parker E Deal, et al. Kiloherz frame-rate two-photon tomography. *Nature methods*, 16(8):778–786, 2019.
- Yunyang Li, Shu Guo, Ben Mattison, Junjie Hu, Kwun Nok Mimi Man, and Weijian Yang. High-speed two-photon microscopy with adaptive line-excitation. 11(8):1138, 2024. ISSN 2334-2536. doi: 10.1364/OPTICA.529930. URL <https://opg.optica.org/abstract.cfm?URI=optica-11-8-1138>.
- Rongwen Lu, Wenzhi Sun, Yajie Liang, Aaron Kerlin, Jens Bierfeld, Johannes D Seelig, Daniel E Wilson, Benjamin Scholl, Boaz Mohar, Masashi Tanimoto, et al. Video-rate volumetric functional imaging of the brain at synaptic resolution. *Nature neuroscience*, 20(4):620–628, 2017.
- Ben Mattison, Shing-Jiuan Liu, Feng Tian, and Weijian Yang. High speed miniaturized multiphoton microscopy with elliptical beam excitation. In *Optics and the Brain*, pages JT4B–33. Optica Publishing Group, 2023.

- Xuelong Mi, Alex Bo-Yuan Chen, Daniela Duarte, Erin Carey, Charlotte R Taylor, Philipp N Braaker, Mark Bright, Rafael G Almeida, Jing-Xuan Lim, Virginia MS Ruetten, et al. Fast, accurate, and versatile data analysis platform for the quantification of molecular spatiotemporal signals. *bioRxiv*, 2024.
- Gal Mishne and Adam Charles. Deep and shallow data science for multi-scale optical neuroscience. In *Neural Imaging and Sensing 2024*, volume 12828, page 1282802. SPIE, 2024.
- Gal Mishne and Adam S Charles. Learning spatially-correlated temporal dictionaries for calcium imaging. In *ICASSP 2019-2019 IEEE International Conference on Acoustics, Speech and Signal Processing (ICASSP)*, pages 1065–1069. IEEE, 2019.
- Eran A. Mukamel, Axel Nimmerjahn, and Mark J. Schnitzer. Automated analysis of cellular signals from large-scale calcium imaging data. 63(6):747–760, 2009. ISSN 08966273. doi: 10.1016/j.neuron.2009.08.009. URL <https://linkinghub.elsevier.com/retrieve/pii/S0896627309006199>.
- Alexander Song, Adam S Charles, Sue Ann Koay, Jeff L Gauthier, Stephan Y Thiberge, Jonathan W Pillow, and David W Tank. Volumetric two-photon imaging of neurons using stereoscopy (vtwins). *Nature methods*, 14(4):420–426, 2017.
- Alexander Song, Jeff L Gauthier, Jonathan W Pillow, David W Tank, and Adam S Charles. Neural anatomy and optical microscopy (naomi) simulation for evaluating calcium imaging methods. *Journal of neuroscience methods*, 358:109173, 2021.
- Jianglai Wu, Na Ji, and Kevin K. Tsia. Speed scaling in multiphoton fluorescence microscopy. 15(11):800–812, 2021. ISSN 1749-4885, 1749-4893. doi: 10.1038/s41566-021-00881-0. URL <https://www.nature.com/articles/s41566-021-00881-0>.